THE JOURNAL OF PHYSICAL CHEMISTRY C

Article

pubs.acs.org/JPCC

Atomic Layer Deposition of AlF_3 Using Trimethylaluminum and Hydrogen Fluoride

Younghee Lee,[†] Jaime W. DuMont,[†] Andrew S. Cavanagh,[†] and Steven M. George*[,†,‡]

[†]Department of Chemistry and Biochemistry and [‡]Department of Mechanical Engineering, University of Colorado at Boulder, Boulder, Colorado 80309, United States

ABSTRACT: The atomic layer deposition (ALD) of AlF_3 was demonstrated using trimethylaluminum (TMA) and hydrogen fluoride (HF). The HF source was HF-pyridine. In situ quartz crystal microbalance (QCM), quadrupole mass spectrometer (QMS), and Fourier transform infrared (FTIR) spectroscopy measurements were used to study AlF_3 ALD. The AlF_3 ALD film growth was examined at temperatures from 75 to 300 °C. Both the TMA and HF reactions displayed self-limiting behavior. The maximum mass gain per cycle (MGPC) of 44 ng/(cm^2 cycle) for AlF_3 ALD occurred at 100 °C. The MGPC values decreased at higher temperatures. The MGPC values were negative at T > 250 °C when TMA and HF were able to etch the AlF_3 films. Film thicknesses were also determined using ex situ X-ray reflectivity (XRR) and spectroscopic ellipsometry (SE) measurements. The AlF_3 ALD growth rate determined by the ex situ analysis was 1.43 Å/cycle at 100 °C. These ex situ measurements were in excellent agreement with the in situ QCM measurements. FTIR analysis monitored the growth of infrared absorbance from Al−F stretching vibrations at 500−900 cm^{-1} during AlF_3 ALD. In addition, absorption peaks were observed that were consistent with $AlF(CH_3)_2$ and HF species on the surface after the TMA and HF exposures, respectively. X-ray photoelectron spectroscopy (XPS) and Rutherford backscattering spectrometry (RBS) measurements revealed that the deposited films were nearly stoichiometric AlF_3 with an oxygen impurity of only ~2 at %. AlF_3 ALD may be useful for a number of applications such as ultraviolet optical films, protective coatings for the electrodes of Li ion batteries, and Lewis acid catalytic films.

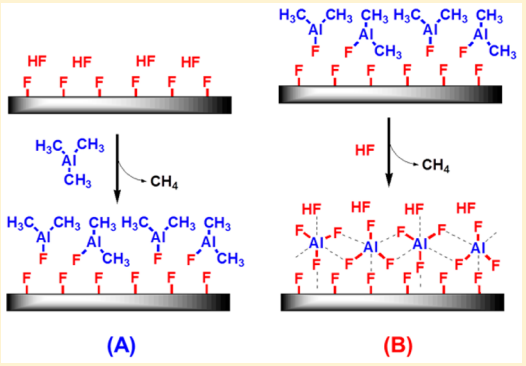

I. INTRODUCTION

Aluminum fluoride (AlF_3) is a dielectric material with a low refractive index[1,2] and wide band gap >10 eV.[3,4] AlF_3 has high transmission at infrared (IR), ultraviolet (UV), and deep UV wavelengths.[1,5−7] These properties make AlF_3 useful for optical coatings. AlF_3 has also been demonstrated as an excellent protective film for Li ion batteries.[8,9] AlF_3 films enhance the cycling stability of anode and cathode materials[8−10] and also improve the thermal stability by suppressing exothermal side reactions.[11] In addition, AlF_3 is employed as a heterogeneous catalyst for the production of chlorofluorocarbons (CFCs) due to its strong Lewis acidity.[12−14]

AlF_3 films have been grown by physical vapor deposition techniques such as sputtering,[15,16] thermal evaporation,[3,6,17] electron beam deposition,[1,5] and ion-assisted deposition.[18] AlF_3 films have also been grown by atomic layer deposition (ALD). ALD is a technique based on sequential, self-limiting surface reactions that deposits extremely conformal and continuous thin films with atomic level control.[19] We initially reported AlF_3 ALD using trimethylaluminum (TMA) and HF from a HF-pyridine solution.[20] AlF_3 ALD has also been demonstrated recently using a halide−halide exchange reaction with $AlCl_3$ and TiF_4.[21]

In this paper, the growth of AlF_3 ALD films using TMA and HF as the reactants was examined using in situ quartz crystal microbalance (QCM), quadrupole mass spectrometer (QMS), and Fourier transform infrared (FTIR) spectroscopy measurements. The reactions were performed at temperatures between 75 and 300 °C. The AlF_3 film thickness and density were determined with ex situ X-ray reflectivity (XRR). The AlF_3 film thickness and refractive index were measured with spectroscopic ellipsometry (SE). The structure of the AlF_3 films was examined with grazing incidence X-ray diffraction (GIXRD). The composition of the AlF_3 ALD film was also determined with X-ray photoelectron spectroscopy (XPS) and Rutherford backscattering spectrometry (RBS).

This study focuses on the fundamental growth mechanism of AlF_3 ALD films. These mechanistic studies are important to understand the basis of ALD growth rates. Too often the ALD community assumes that there must be an ideal "ALD window" where the growth rate is constant over a range of temperatures.[19] In reality, the ALD growth rate is always dependent on the underlying surface chemistry. The surface species and surface reactions can change with temperature and lead to varying ALD growth rates. This situation is particularly true for

Received: March 18, 2015
Revised: May 22, 2015
Published: May 27, 2015

DOI: 10.1021/acs.jpcc.5b02625
J. Phys. Chem. C 2015, 119, 14185−14194

AlF_3 ALD, where etching reactions can yield negative growth rates at higher temperatures.

II. EXPERIMENTAL SECTION

A. Viscous Flow Reactor with in Situ QCM and QMS. The ALD reactions were performed at temperatures between 75 and 300 °C in a viscous flow ALD reactor equipped for in situ QCM and QMS measurements.[22,23] A mechanical pump (Pascal 2015SD, Alcatel) was used to maintain vacuum conditions in the ALD reactor. Reactants were dosed into a N_2 carrier gas. A mass flow controller (Type 1179A, MKS) supplied a constant N_2 carrier gas flow of 150 sccm. This N_2 gas flow resulted in a base pressure of ~1 Torr in the reactor. A PID temperature controller (2604, Eurotherm) kept the reactor at a fixed temperature within ±0.04 °C. A bakeable capacitance manometer (Baratron 121A, MKS) monitored pressure change during the reactions.

The AlF_3 ALD reactions were performed using TMA (97%, Sigma-Aldrich) and HF-pyridine (70 wt % HF, Sigma-Aldrich) as the reactants. Pure anhydrous HF from a gas cylinder has also been employed recently for MgF_2 ALD.[24] Use of gaseous HF from HF-pyridine enables the safe handling of anhydrous HF. HF-pyridine is a liquid at room temperature and is known as Olah's reagent.[25] HF-pyridine was transferred to a stainless steel bubbler in a dry N_2-filled glovebag.

The HF-pyridine solution has an equilibrium with gaseous HF. Our mass spectrometer measurements have revealed that HF is the dominant species in the vapor pressure of HF-pyridine. With static exposures and no pumping on our ALD reactor, the vapor pressure of HF from the HF-pyridine solution was 90−100 Torr at room temperature. Each AlF_3 ALD experiment was conducted on a fresh Al_2O_3 ALD film. The Al_2O_3 ALD films were prepared using TMA and H_2O (Chromasolv for HPLC, Sigma-Aldrich). The Al_2O_3 ALD films were grown using at least 100 Al_2O_3 ALD cycles.

The TMA, HF-pyridine, and H_2O precursors were held at room temperature. Unreacted HF leaving the reactor was removed by bubbling the gas exhaust stream through a calcium oxide solution. This calcium oxide solution was located immediately after the mechanical pump. An activated alumina trap (Visi-Trap, LACO Technologies) located on the inlet of the mechanical pump also helped remove HF from the exhaust stream.

A film deposition monitor (Maxtek TM-400, Inficon) was used to perform the in situ QCM measurements. The QCM sensors were polished, 6 MHz, AT-cut (Colorado Crystal Corp.) and RC-cut (Colnatec) quartz crystals with gold electrodes. The QCM sensor was secured in a bakeable single sensor head (BSH-150, Inficon) and sealed with high-temperature epoxy (Epo-Tek H21D, Epoxy Technology). Deposition on the back-side of the QCM sensor was prevented by flowing an additional 20 sccm of N_2 through the QCM housing.[22] This additional N_2 was supplied using a bellows-sealed metering valve (SS-4BMG, Swagelok).

Quadrupole mass spectrometry (QMS) was performed on the vapor phase species in the ALD reactor. These measurements utilized a residual gas analyzer (RGA 200, Stanford Research Systems). The reactant and product gases during the ALD reactions were sampled using an aperture with a diameter of 50 μm. The aperture separated the pressure in the ALD reactor at ~1 Torr from the pressure in the QMS region at ~1 × 10^{-7} Torr. To maintain these pressures with a conductance between the two regions, the QMS region was differentially pumped with a turbomolecular pump (V70LP, Varian). A dual thoriated/iridium (ThO_2/Ir) filament was used for electron emission in the ionizer of the mass spectrometer. The ionization energy was 70 eV. A Faraday cup was used as the ion detector.

B. Fourier Transform Infrared (FTIR) Spectroscopy. The in situ FTIR studies were performed in a separate reactor equipped with an FTIR spectrometer that has been described previously.[26] The reactor was pumped using a mechanical pump (TRIVAC D8B, Oerlikon Leybold Vacuum). The FTIR spectrometer (Nicolet 6700 FTIR, Thermo Scientific) utilized a liquid-N_2-cooled mercury cadmium telluride (MCT-B) detector. Dry, CO_2-free air was employed to purge the spectrometer, mirror, and detector setup. Each spectrum consisted of a total of 100 scans at 4 cm^{-1} resolution from 400 to 4000 cm^{-1}.

The transmission FTIR measurements were performed on high surface area SiO_2 nanoparticles (99.5%, U.S. Research Nanomaterials) with an average diameter of 15−20 nm. The high surface area of these nanoparticles was needed to enhance the number of surface species in the infrared beam. The SiO_2 nanoparticles absorb infrared radiation between 400 and 650 cm^{-1}, 700−875 cm^{-1}, and 925−1400 cm^{-1}. These absorption regions leave available windows to observe absorbance from the AlF_3 ALD film. Sample preparation involved pressing the SiO_2 nanoparticles into a tungsten grid support (Tech-Etch).[27,28] The tungsten grids had dimensions of 2 cm × 3 cm. Each grid was 50 μm thick with 100 grid lines per inch.

The tungsten grid was resistively heated using a DC power supply (6268B, 20 V/20 A, Hewlett-Packard). The voltage output of the power supply was controlled by a PID temperature controller (Love Controls 16B, Dwyer Instruments). A type K thermocouple was attached to the bottom of the tungsten grid with epoxy (Ceramabond 571, Aremco) that attached and electrically isolated the thermocouple.

The AlF_3 ALD reactions were performed using sequential exposures of TMA (97%, Sigma-Aldrich), and HF from HF-pyridine (70 wt % HF, Sigma-Aldrich). The AlF_3 ALD films were deposited using TMA doses with exposure times of 1.0 s and HF doses with exposure times of 1.0 s. These exposure times produced pressure transients of ~350 mTorr above the base pressure for TMA and HF, respectively. A 240 s purge time was utilized after each reactant exposure.

Reactants were dosed into the flowing N_2 carrier gas stream. A mass flow controller supplied the constant N_2 carrier gas flow rate of 150 sccm. This N_2 gas flow resulted in a base pressure of ~1.650 Torr in the reactor. The TMA and HF-pyridine were held at room temperature. Like the HF abatement procedure employed during the QCM experiments, the excess HF leaving the reactor was removed using an activated alumina trap and by bubbling the gas exhaust stream through a calcium oxide solution.

C. Ex Situ Film Characterization using XRR, XRD, and SE. For ex situ measurements, boron-doped Si (100) wafers (p-type, Silicon Valley Microelectronics) were used as the substrates. The Si wafer was cleaved into samples with dimensions of 2.5 cm by 2.5 cm. These samples were cleaned with acetone, isopropanol, and deionized water and dried with N_2 gas.

The film thicknesses and the density were determined using ex situ XRR measurements. The XRR measurements were performed with a high-resolution X-ray diffractometer (Bede D1, Jordan Valley Semiconductors) using a Cu Kα (λ = 1.540 Å) X-ray tube. The filament current was 35 mA, and the voltage

DOI: 10.1021/acs.jpcc.5b02625
J. Phys. Chem. C 2015, 119, 14185−14194

was 40 kV. The step size and acquisition time for all the XRR scans were 10 arcsec and 5 s, respectively. The XRR scans were modeled with the Bede REFS software package (Bede REFS, Jordan Valley Semiconductors) to determine film thickness, surface roughness, and film density. The film structure was examined by grazing incidence X-ray diffraction (GIXRD) using the same X-ray diffractometer.

The film thicknesses and refractive indices were measured using spectroscopic ellipsometry (SE). These measurements were performed using a spectroscopic ellipsometer (M-2000, J. A. Woollam) employing a spectral range from 240 to 1700 nm with an incidence angle of 75°. Measurement of Ψ and Δ were modeled with the CompleteEASE software package (CompleteEASE, J. A. Woollam) and a Sellmier model.[29] The Sellmeier model is commonly used for optically transparent films such as metal fluoride films.[29]

D. X-ray Photoelectron Spectroscopy and Rutherford Backscattering Spectrum. The film composition was determined by X-ray photoelectron spectroscopy (XPS). The XPS instrument (PHI 5600, RBD Instruments) used a monochromatic Al Kα X-ray source (1486.6 eV). Survey scans were measured with a pass energy of 93.9 eV and a step size of 0.400 eV. Depth profiles were obtained using Ar ion sputtering. A pass energy of 58.7 eV and a step size of 0.250 eV were used for the depth profiling analysis. An electron beam neutralizer was employed at 17.8 mA. Data was collected with the Auger Scan software package (Auger Scan, RBD Instruments) and analyzed with the Casa XPS software package (Casa XPS, Casa Software).

The RBS analysis was performed in the Nanofabrication Center at the University of Minnesota. Glassy carbon plates (type 2, 1 mm thick, Alfa Aesar) with dimensions of 1.2 cm × 1.2 cm were used as the substrates for RBS analysis. The glassy carbon substrates were cleaned with acetone, isopropanol, and deionized water and dried with N_2 gas. Initially, Al_2O_3 ALD films were deposited as an adhesion layer on the glassy carbon plates using 20 cycles of Al_2O_3 ALD. The AlF_3 films were then deposited using 800 AlF_3 ALD cycles at 150 °C.

The incident 2 MeV beam of He^+ ions was integrated to 40 μC of total charge per point using an ion detector positioned at 165° relative to the incident ion beam. The backscattered ions were collected using a microchannel plate detection system. RBS spectra were acquired using a MAS 1700 pelletron tandem ion accelerator (5SDH) equipped with charge exchange RF plasma source (National Electrostatics Corporation) and RBS 400 analytical endstation (Charles Evans & Associates). The data was modeled using the QUARK software package.[30]

III. RESULTS AND DISCUSSION

A. Growth of AlF_3 Films. Figure 1 shows the QCM measurements of mass gain during 200 cycles of AlF_3 ALD at 150 °C using TMA and HF. The initial layer on the QCM sensor was an Al_2O_3 ALD film grown with 200 cycles of Al_2O_3 ALD using TMA and H_2O as the reactants. The reaction sequence of one AlF_3 ALD cycle consisted of a 1 s dose of TMA, 30 s of N_2 purge, a 1 s dose of HF, and 30 s of N_2 purge. This reaction sequence is designated as (1−30−1−30). The TMA and HF doses produced pressure transients of 40 and 100 mTorr, respectively. The AlF_3 ALD growth is very linear with a mass gain per cycle (MGPC) of 31 ng/(cm^2 cycle). In addition, AlF_3 ALD nucleates nearly immediately on the initial Al_2O_3 ALD surface.

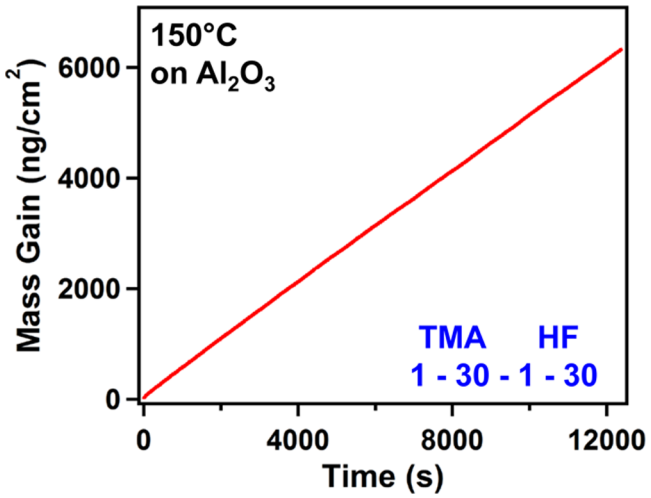

Figure 1. Mass gain versus time during 200 AlF_3 ALD cycles with TMA and HF as the reactants on Al_2O_3 at 150 °C using the reaction sequence of (1−30−1−30).

Figure 2 shows the mass gain during three sequential AlF_3 ALD cycles at 150 °C using the reaction sequence (1−30−1−30). These three cycles were the 148th, 149th, and 150th AlF_3 ALD cycles in Figure 1. The mass gains are very distinct. The mass increase after the TMA exposure is ΔM_{TMA} = 22 ng/(cm^2 cycle). The mass increase after the HF exposure is ΔM_{HF} = 9 ng/(cm^2 cycle). The MGPC was 31 ng/(cm^2 cycle).

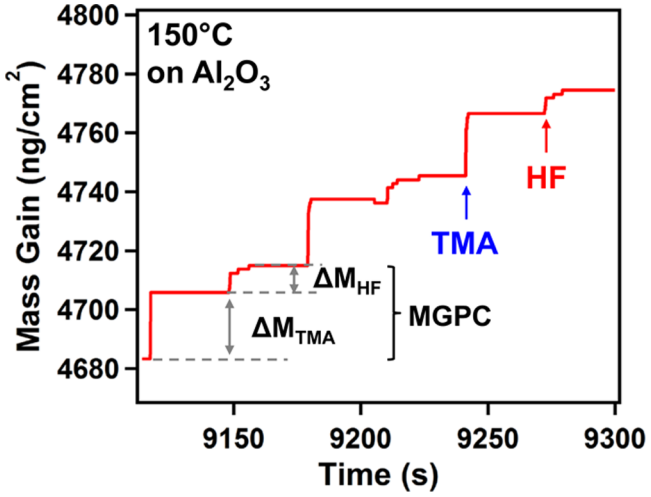

Figure 2. Enlargement of mass gain versus time for three sequential TMA and HF exposures during AlF_3 ALD in the steady-state, linear growth regime shown in Figure 1.

Figure 3 displays the MGPC and the ΔM_{TMA}/MGPC ratio during 200 cycles of AlF_3 ALD using a reaction sequence of (1−30−1−30). The MGPC is 31 ng/(cm^2 cycle) and consists of constant mass gains of ΔM_{TMA} = 22 ng/(cm^2 cycle) and ΔM_{HF} = 9 ng/(cm^2 cycle). Except for the first 3 AlF_3 ALD cycles, the ΔM_{TMA}/MGPC ratio is constant at 0.71. The MGPC and the ΔM_{TMA}/MGPC ratio were nearly independent of the purge time. Extended purge times of 120 s slightly decreased the MGPC to ~29 ng/(cm^2 cycle). However, the ΔM_{TMA}/MGPC ratio remained at 0.71. The ΔM_{TMA}/MGPC ratio will be used later to determine the reaction stoichiometry.

DOI: 10.1021/acs.jpcc.5b02625
J. Phys. Chem. C 2015, 119, 14185−14194

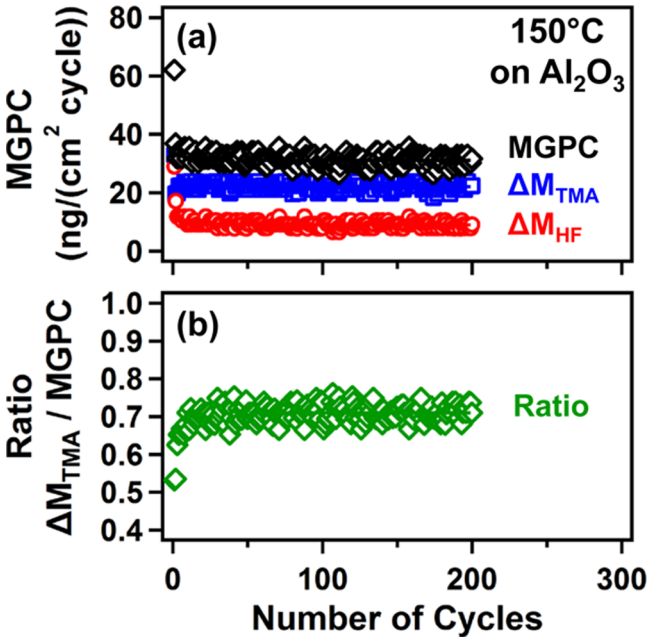

Figure 3. (a) MGPC, ΔM_{TMA}, and ΔM_{HF} and (b) M_{TMA}/MGPC ratio during 200 AlF_3 ALD cycles with TMA and HF as the reactants on Al_2O_3 at 150 °C.

The self-limiting behavior of the TMA and HF reactions for AlF_3 ALD was also examined using in situ QCM experiments. Figure 4 (panels a and b) shows the mass gains during the TMA and HF exposures, respectively, at 150 °C. For each of these exposures, the other reactant exposure had reached saturation. Each minidose consisted of an exposure time of 0.5 s and a purge time of 30 s. Both reactions displayed self-limiting behavior. ΔM_{TMA} versus minidoses of TMA reached the plateau of ΔM_{TMA} = ~22 ng/(cm^2 cycle) after one minidose. Similarly, ΔM_{HF} versus minidoses of HF leveled off at ΔM_{HF} = ~9 ng/(cm^2 cycle) after one minidose.

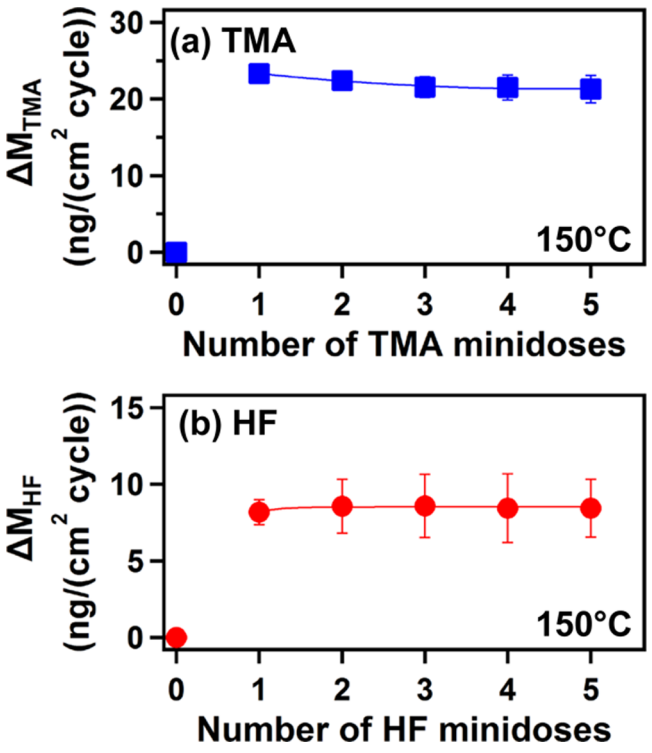

Figure 4. (a) ΔM_{TMA} versus number of TMA minidoses at 150 °C with the HF exposure fixed at 1.0 s. (b) ΔM_{HF} versus number of HF minidoses at 150 °C with the TMA exposure fixed at 1.0 s.

Figure 5 displays the film thickness for 20, 50, 100, 200, 400, and 800 cycles of AlF_3 ALD on a Si wafer at 150 °C as determined by ex situ XRR and SE analysis. The thickness measurements from XRR and SE were nearly identical. The AlF_3 ALD growth on the silicon wafers was linear with a growth rate of 1.0 Å/cycle at 150 °C. The density of these AlF_3 ALD films obtained from XRR was 2.9 g/cm^3. This density is slightly less than the bulk density of 3.10 g/cm^3 for crystalline AlF_3.[31] AlF_3 ALD films grown using $AlCl_3$ and TiF_4 as the reactants also observed a density of 2.8−2.9.[21]

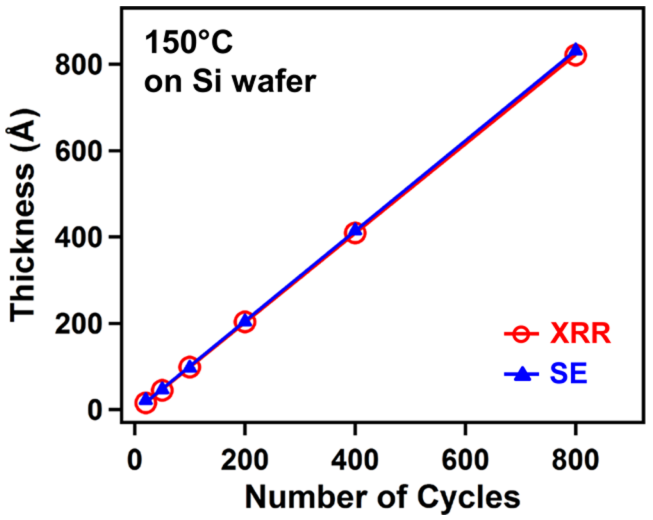

Figure 5. Film thickness versus number of cycles for 800 AlF_3 ALD cycles with TMA and HF as the reactants on Si(100) at 150 °C determined by XRR and SE measurements.

The growth rate of 1.0 Å/cycle at 150 °C obtained by the XRR analysis can be compared with the MGPC of 31 ng/(cm^2 cycle) obtained by the QCM measurements. This comparison is possible using the density of 2.9 g/cm^3 obtained by XRR analysis. With the use of this density, the MGPC of 31 ng/(cm^2 cycle) is equivalent to a growth rate of 1.1 Å/cycle. There is excellent agreement between the AlF_3 ALD growth rates determined using QCM and XRR measurements.

Figure 6 reveals some of the gas phase species detected by the quadrupole mass spectrometer during AlF_3 ALD using sequential TMA and HF exposures at 150 °C. These mass spectrometry signals were recorded at the same time as the mass gains shown in Figure 2. The targeted gas phase species were the CH_4 reaction product at m/z = 16, the HF reactant at m/z = 20, and the pyridine species at m/z = 52. Results are shown for three AlF_3 ALD cycles using the reaction sequence (1−30−1−30).

The mass signal at m/z = 16 in Figure 6 indicates that the CH_4 reaction product appears during both the TMA and HF exposures. HF reacts with Al-CH_3* surface species to produce CH_4. TMA also reacts with HF on the surface to produce CH_4. Some of the m/z = 16 mass signal is attributed to cracking fragments of TMA. Mass spectrometer analysis was performed after the TMA reaction reached saturation. This analysis showed that cracking of TMA could account for ~1/3 of the

DOI: 10.1021/acs.jpcc.5b02625
J. Phys. Chem. C 2015, 119, 14185−14194

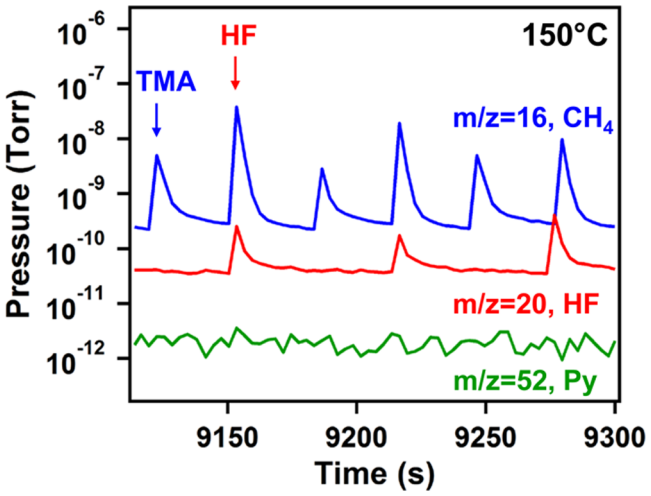

Figure 6. Mass spectrometer signals for m/z = 16, 20, and 52 for CH_4, HF, and pyridine, respectively, during three AlF_3 ALD cycles at 150 °C. These signals were recorded at the same time as the mass changes shown in Figure 2.

m/z = 16 mass signal observed in Figure 6 during TMA exposures.

Figure 6 also indicates that a mass signal at m/z = 20 is coincident only with the HF exposures. This mass signal is assigned to the HF reactant. The QMS does not detect a mass signal at m/z = 52 or m/z = 79. These mass signals are the two largest mass cracking fragments for pyridine.[32] These results indicate that the HF-pyridine solution has a negligible pyridine vapor pressure. In contrast, the vapor pressure of pyridine at 20 °C is ∼15 Torr.[33] The negligible pyridine vapor pressure is consistent with the stabilization of pyridine with HF in a high boiling point azeotrope.[34] Additional experiments with pure pyridine solutions clearly showed substantial mass signals at m/z = 52 and m/z = 79.

Additional experiments examined the growth of AlF_3 ALD films at various substrate temperatures. Separate experiments were conducted at each substrate temperature after allowing the reactor to stabilize at the desired temperature. Figure 7a shows the temperature dependence of the MGPC from the in situ QCM measurements. The MGPC can be converted to the growth rate in Å/cycle using the film density of 2.9 g/cm^3 measured by XRR. These growth rates are shown in Figure 7b. In addition, Figure 7b also displays the growth rates determined from ex situ XRR and SE measurements. The agreement between the in situ and ex situ measurements of the growth rate is very good. A maximum growth rate of 1.43 Å/cycle was obtained at 100 °C. A summary of the temperature-dependent growth rates is given in Table 1. In comparison, the AlF_3 ALD growth rates are obtained using $AlCl_3$ and TiF_4 as the reactants varied from ∼ 3.2 Å/cycle at 160 °C to ∼0.3 Å/cycle at 300 °C.[21] The contrastive growth rates may be attributed to different growth mechanisms.

Both panels in Figure 7 (panels a and b) show that the AlF_3 ALD growth rate decreases at higher temperatures. The progressive decrease in the AlF_3 ALD growth rate could be explained by the loss of surface species responsible for growth at higher temperature. A similar decrease in ALD growth rate versus temperature was observed for Al_2O_3 ALD.[35] In addition, the AlF_3 ALD growth rate becomes negative at temperatures >250 °C. At these higher temperatures, the TMA and HF exposures are able to etch the AlF_3 ALD films. Separate

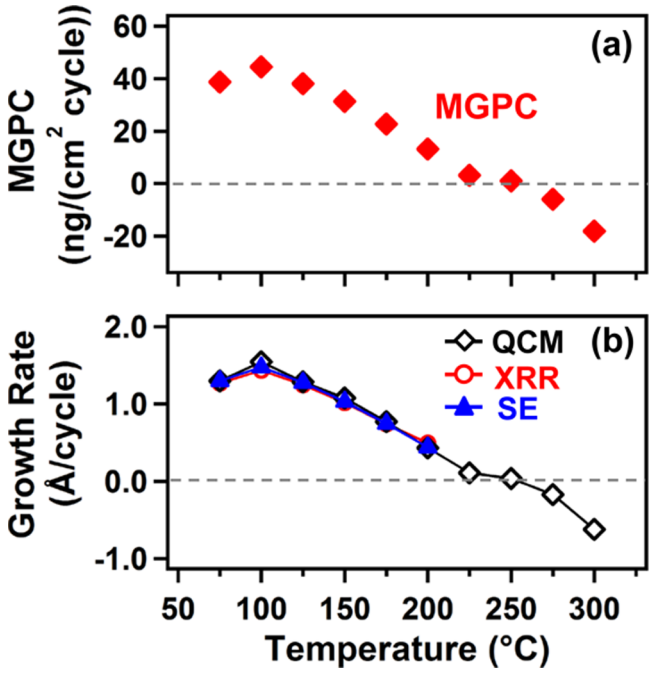

Figure 7. (a) Mass gain per cycle (MGPC) and (b) growth rate versus reaction temperature using reaction sequence of (1−30−1−30).

Table 1. ΔM_{TMA}, ΔM_{HF}, MGPC, ΔM_{TMA}/MGPC, and x for AlF_3 ALD at different temperatures. MGPC, ΔM_{TMA}, and ΔM_{HF} are in units of ng/(cm^2 cycle). Growth rate is in units of Å/cycle.

temperature (°C)	MGPC	growth rate	ΔM_{TMA}	ΔM_{HF}	ΔM_{TMA}/MGPC	x
75	38.7	1.27	28.3	10.4	0.73	0.67
100	44.4	1.43	29.7	14.8	0.67	0.99
125	38.1	1.25	26.2	12.0	0.69	0.88
150	31.4	1.02	22.3	9.1	0.71	0.78
175	22.7	0.74	16.7	6.0	0.73	0.67
200	13.2	0.50	9.3	3.9	0.70	0.83

experiments confirmed that the etching occurred during the TMA exposures.

The AlF_3 etching is very intriguing and may occur by the reaction: $AlF_3 + 2Al(CH_3)_3 \rightarrow 3AlF(CH_3)_2$. In this reaction, TMA accepts fluorine from AlF_3 to form $AlF(CH_3)_2$. The $-CH_3$ from TMA is transferred to the substrate and forms additional $AlF(CH_3)_2$. At lower temperatures, $AlF(CH_3)_2$ may remain on the surface and lead to AlF_3 ALD growth during the HF exposure. At higher temperature, $AlF(CH_3)_2$ may desorb and yield AlF_3 etching during the TMA exposure. Additional mass spectrometry experiments are planned to confirm the presence of $AlF(CH_3)_2$ in the gas phase at higher temperatures.

This etching process is related to the thermal atomic layer etching (ALE) of Al_2O_3 and HfO_2 films that has been observed using $Sn(acac)_2$ and HF reactants.[36,37] However, in this case, the etching of AlF_3 by TMA is not self-limiting. The AlF_3 etching at 250−300 °C is dependent on the length of the TMA exposure. We will report on AlF_3 ALE using $Sn(acac)_2$ and HF in a future publication.

B. Reaction Mechanism for AlF_3 ALD. FTIR vibrational spectroscopy was used to monitor AlF_3 ALD and identify the surface species present during AlF_3 ALD. Figure 8 shows the growth of absorbance in the frequency range from 500 to 900

DOI: 10.1021/acs.jpcc.5b02625
J. Phys. Chem. C 2015, 119, 14185−14194

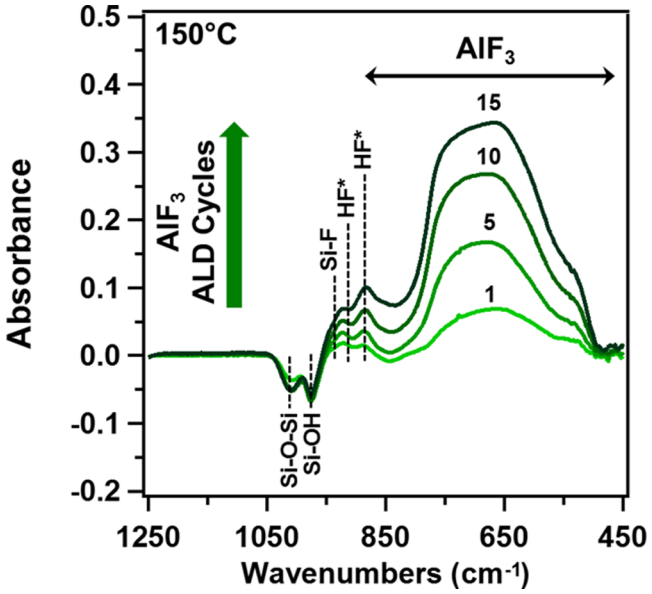

Figure 8. FTIR spectra vs AlF_3 ALD cycles on the initial SiO_2 nanoparticles at 150 °C. These spectra are all referenced to the SiO_2 nanoparticles.

cm^{-1} during AlF_3 ALD cycles on SiO_2 nanoparticles at 150 °C. These FTIR spectra were recorded after HF exposures and are referenced to the FTIR spectrum of the initial SiO_2 nanoparticles. The absorbance progressively increases versus number of AlF_3 ALD cycles. The growth of absorbance in the frequency range from 500 to 900 cm^{-1} is attributed to the Al−F stretching vibration in amorphous AlF_3. Earlier vibrational studies have observed the absorption of Al−F stretching vibrations in amorphous AlF_3 at 500−900 cm^{-1}.[17,38−40]

Figure 8 also shows absorbance losses at 975 and 1010 cm^{-1} as well as absorbance gains at 880, 920, and 930 cm^{-1}. The absorbance losses at 975 and 1010 cm^{-1} are assigned to the removal of Si−OH and Si−O−Si species on the initial SiO_2 substrate, respectively. This loss has been observed during reactions of TMA with silanol and siloxane surface species to form surface Si−O−$Al(CH_3)_2$ groups.[41] The positive feature at 930 cm^{-1} is attributed to the formation of Si−F bonds, while the positive features at 880 and 920 cm^{-1} are assigned to HF molecules that are adsorbed on the surface.[42−44]

Figure 9 shows the FTIR difference spectra for two consecutive TMA and HF exposures at 150 °C. These difference spectra are referenced to the spectra after the previous reactant exposure. Figure 9a shows the difference spectrum after the TMA exposure referenced to the spectrum after the previous HF exposure (TMA-HF). This difference spectrum has been displaced for clarity in presentation. Figure 9a reveals a prominent absorbance gain at 725 cm^{-1} and smaller absorbance gains at ∼600−650 and ∼2800−3000 cm^{-1}. These positive absorbance features are all consistent with the vibrational features of molecular $AlF(CH_3)_2$.[45] The prominent absorbance feature at 725 cm^{-1} is assigned to the CH_3 rocking mode of $AlF(CH_3)_2$.[45] The absorbance feature at 600−650 cm^{-1} is attributed to the Al−F stretching mode of $(CH_3)_2AlF$.[45] The positive features between 2800 and 3000 cm^{-1} are consistent with the C−H stretches of $AlF(CH_3)_2$.[45]

The TMA exposure also results in negative features at 900 and ∼3000−3675 cm^{-1} that are attributed to the removal of HF surface species. The negative feature at 900 cm^{-1} is

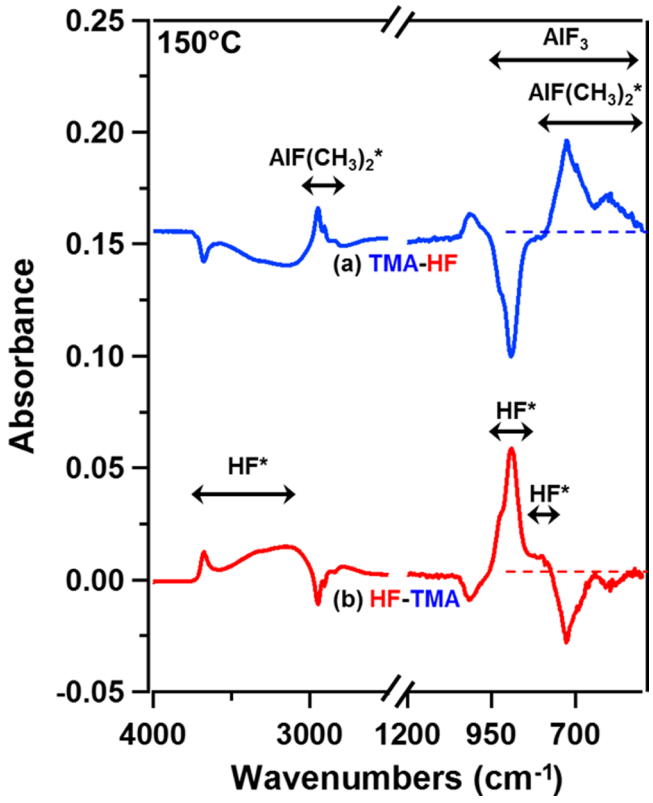

Figure 9. FTIR difference spectra during AlF_3 ALD at 150 °C. (a) Difference spectrum after the TMA exposure referenced to the spectrum after the previous HF exposure (TMA-HF) and (b) difference spectrum after the HF exposure referenced to the spectrum after the previous TMA exposure (HF-TMA).

assigned to an out-of-plane librational (reciprocating) HF mode.[42] The absorbance features at ∼3000−3675 cm^{-1} are consistent with the stretching vibrations of isolated and hydrogen-bonded Al-(HF)* surface species absorbed on AlF_3 surfaces, respectively.[46]

Figure 9b displays the difference spectrum after the HF exposure referenced to the spectrum after the previous TMA exposure (HF-TMA). Most of the absorbance features that were added as a result of the previous TMA exposure are removed by the subsequent HF exposure. Negative absorbance features at 725 and 2800−3000 cm^{-1} are consistent with the removal of the $AlF(CH_3)_2$* surface species.[45] Positive absorbance features at 900 and ∼3000−3675 cm^{-1} also indicate that HF reabsorbs to the surface.

The dashed lines designate zero absorbance between 500−900 cm^{-1}. The dashed lines help to illustrate that the absorbance gained between 500−900 cm^{-1} during TMA exposures is greater than the absorbance that is lost between 500−900 cm^{-1} during HF exposures. This overall absorbance gain indicates that Al−F species are added during the TMA and HF exposures. The bulk AlF_3 vibrational mode between 500−900 cm^{-1} grows steadily with the number of reaction cycles as shown in Figure 8.

On the basis of the results from the QCM and FTIR measurements, Figure 10 presents a schematic showing the proposed reaction mechanism for AlF_3 ALD. In reaction A, TMA molecules react with HF molecules adsorbed on the surface to yield $AlF(CH_3)_2$ and CH_4 molecules as the reaction products. The $AlF(CH_3)_2$ species remain adsorbed on the

DOI: 10.1021/acs.jpcc.5b02625
J. Phys. Chem. C 2015, 119, 14185−14194

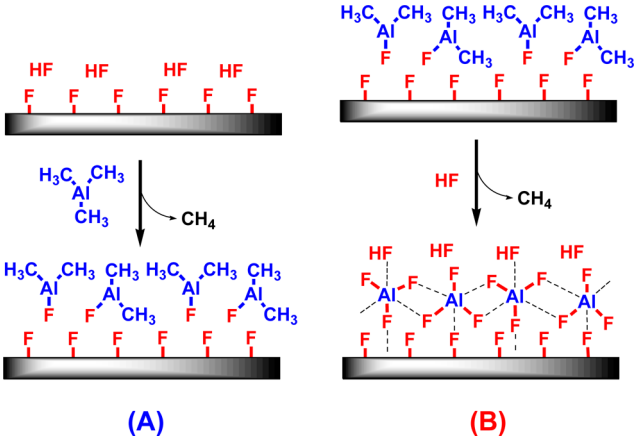

Figure 10. Proposed reaction mechanism for AlF_3 ALD using TMA and HF as the reactants.

surface. Note that the desorption of the $AlF(CH_3)_2$ species would have led to AlF_3 etching. In reaction B, HF converts the adsorbed $AlF(CH_3)_2$ species to AlF_3. The AlF_3 film is expected to form octahedral Al centers with bridging fluorines. CH_4 is again a reaction product and additional HF molecules may remain on the surface.

The more general surface chemistry for AlF_3 ALD can be expressed by

$$\text{(A) } AlF_3|xHF^* + Al(CH_3)_3 \rightarrow AlF_3|AlF_x(CH_3)_{3-x}^* + xCH_4 \quad (2)$$

$$\text{(B) } AlF_3|AlF_x(CH_3)_{3-x}^* + 3HF \rightarrow AlF_3|AlF_3|xHF^* + (3-x)CH_4 \quad (3)$$

The asterisks designate the surface species. The vertical lines distinguish the various surface species. The parameter x quantifies the number of HF molecules adsorbed on the surface relative to the number of AlF_3 species deposited during one AlF_3 ALD cycle. $x = 1$ indicates one HF per AlF_3 on the surface as shown in Figure 10. $x = 1$ is also consistent with $AlF(CH_3)_2$ as the adsorbed surface species in Figure 10.

On the basis of this surface chemistry, the ΔM_{TMA}/MGPC ratio can be determined by

$$\frac{\Delta M_{TMA}}{MGPC} = \frac{\Delta M_{TMA}}{\Delta M_{TMA} + \Delta M_{HF}} = \frac{M_{TMA} - x \cdot M_{CH_4}}{M_{TMA} + 3M_{HF} - 3M_{CH_4}} = \frac{M_{TMA} - x \cdot M_{CH_4}}{M_{AlF_3}} \quad (4)$$

In eq 4, M_{TMA}, M_{HF}, M_{CH_4}, and M_{AlF_3} are the molar masses of TMA, HF, CH_4, and AlF_3, respectively. The equation for x is

$$x = \frac{1}{M_{CH_4}}\left[M_{TMA} - M_{AlF_3}\left(\frac{\Delta M_{TMA}}{MGPC}\right)\right] = \frac{1}{16}\left[72.1 - 84.0\left(\frac{\Delta M_{TMA}}{MGPC}\right)\right] \quad (5)$$

The ΔM_{TMA}/MGPC ratio and x can be determined from the mass changes obtained by the QCM measurements. A ΔM_{TMA}/MGPC ratio of 0.71 was determined from the QCM measurements at 150 °C shown in Figure 3. This ratio of 0.71 is close to the ratio of 0.67 based on the proposed mechanism in Figure 10, where $x = 1$.

The ratio varied slightly at the different reaction temperatures. The ΔM_{TMA}/MGPC ratios were 0.73, 0.67, 0.69, 0.71, 0.73 and 0.70 at 75, 100, 125, 150, 175, and 200 °C, respectively. The corresponding x values were 0.67, 0.99, 0.88, 0.78, 0.67, and 0.83 at 75, 100, 125, 150, 175, and 200 °C, respectively. These values are summarized in Table 1. An x value of $x = 0.99$ or nearly $x = 1$ is observed at 100 °C. The maximum AlF_3 ALD growth rate of 1.43 Å/cycle is also measured at 100 °C. x values < 1 are consistent with a mixture of $AlF(CH_3)_2$ and $Al(CH_3)_3$ on the surface after the TMA exposure.

The mass changes measured during the QCM experiments support the existence of HF and $AlF(CH_3)_2$ species on the surface after the HF and TMA exposures. A binding interaction is expected between HF and the AlF_3 surface. Strong coordination of HF on α-AlF_3 and β-AlF_3 surfaces has been predicted by density functional theory (DFT) calculations.[47,48] AlF_3 is a Lewis acid. The F in HF can act as a Lewis base. Together AlF_3 and HF have a strong Lewis acid−base interaction. TMA and $AlF(CH_3)_2$ are also Lewis acids. The F in Al−F* species on the surface can act as a Lewis base. A strong Lewis acid−base interaction is also expected between Al−F* and either TMA or $AlF(CH_3)_2$.

C. Ex Situ AlF_3 Film Characterization. Figure 11 shows an X-ray photoelectron spectroscopy (XPS) sputter depth profile of an AlF_3 ALD film grown at 150 °C. The film is almost entirely aluminum and fluorine after removal of the adventitious surface carbon. Oxygen impurities are detected at ~2 at %. The oxygen impurity may result from water that could be produced in the reaction of HF with metal oxide inside the stainless steel reactor. Carbon and nitrogen impurities are below the detection limit of XPS. The ratio between the calibrated aluminum and fluorine XPS signals is 1:2.4. The preferential sputtering of fluorine may explain the low fluorine signals.[18]

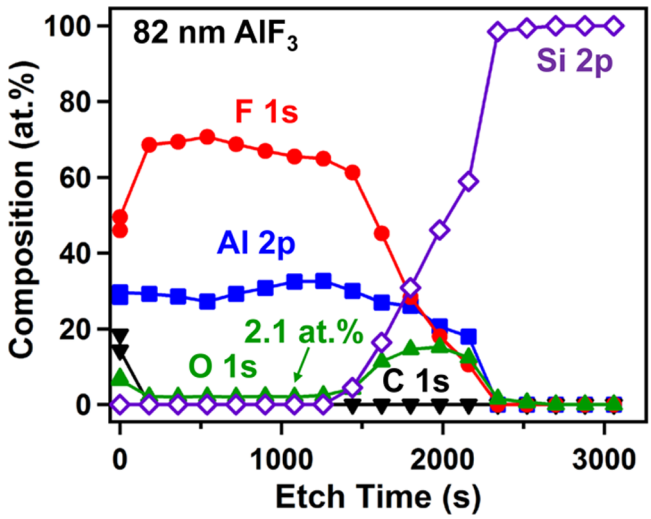

Figure 11. Sputter depth profile of AlF_3 film grown at 150 °C measured by X-ray photoelectron spectroscopy.

Figure 12 shows the Rutherford backscattering spectrum (RBS) of a film grown using 800 AlF_3 ALD cycles at 150 °C. A glassy carbon substrate is used instead of a silicon wafer because aluminum and silicon have similar atomic masses and

DOI: 10.1021/acs.jpcc.5b02625
J. Phys. Chem. C 2015, 119, 14185−14194

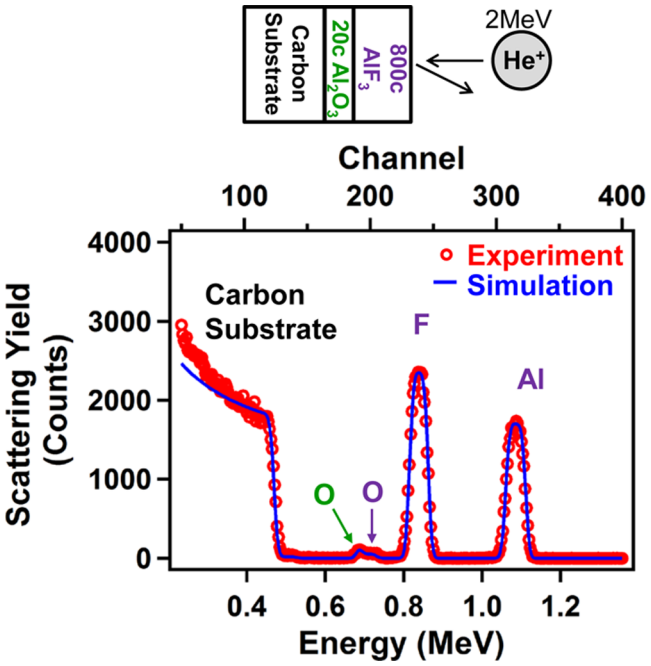

Figure 12. Rutherford backscattering spectrum of AlF_3 film grown at 150 °C using 800 AlF_3 ALD cycles on 20 cycles of Al_2O_3 ALD film on carbon substrate.

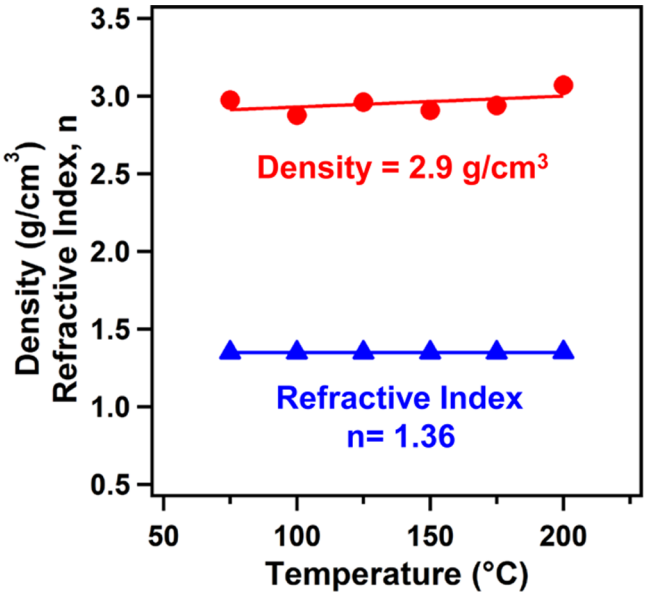

Figure 13. Density and refractive index for AlF_3 ALD films grown at various temperatures.

overlapping RBS signals. An Al_2O_3 ALD film grown on the glassy carbon served as an adhesion layer. The RBS spectrum observed an aluminum peak at 1.1 MeV and a fluorine peak around 0.8 MeV. The aluminum to fluorine ratio is 1:2.85 based on the peak areas. This ratio is consistent with nearly stoichiometric AlF_3. Carbon or nitrogen is not observed in the film within the detection limits of RBS.

Grazing incidence X-ray diffraction (GIXRD) analysis revealed that the AlF_3 ALD films were amorphous. The AlF_3 ALD films remain amorphous even after annealing at 500 °C in argon. AlF_3 ALD film roughnesses of 4−5 Å were measured by XRR analysis at all the reaction temperatures. These smooth films are consistent with amorphous AlF_3 ALD films. AlF_3 films grown by physical vapor deposition (PVD) techniques have been amorphous.[6,15,17,49] AlF_3 films deposited by PVD and annealed at 350 °C were also amorphous.[6] In addition, amorphous AlF_3 ALD films were grown using $AlCl_3$ and TiF_4 as the reactants except at the highest growth temperature of 340 °C.[21]

The film density and refractive index was also measured for AlF_3 films grown using 200 AlF_3 ALD cycles at different temperatures. These results are presented in Figure 13. The film density is nearly constant at 2.9 g/cm^3 at all reaction temperatures. This density is ∼94% of the bulk density of 3.1 g/cm^3 for crystalline AlF_3.[31] Refractive indices of the films grown at different reaction temperatures are also constant at n = 1.36. These refractive indices were measured by SE at 589 nm and were obtained using the Sellmeier model.

The measured refractive index of n = 1.36 is consistent with n = 1.38 for bulk AlF_3 at 589 nm.[2] The measured refractive index of n = 1.36 is also in agreement with n = 1.36 at 580 nm from AlF_3 ALD films using $AlCl_3$ and TiF_4 as the reactants[21] and n = 1.36 at 600 nm for AlF_3 films grown using electron beam techniques.[1] The extinction coefficient for the AlF_3 films is zero because the AlF_3 ALD films are transparent in the range between 240 and 1700 nm, resulting from the wide band gap of >10 eV for AlF_3.[3,4]

The thickness variation was measured for five samples grown at 150 °C in the reactor at different spatial locations spaced evenly over a length of 5.0 in. using 800 cycles of AlF_3 ALD. The film thicknesses revealed good spatial uniformity within ±1% as measured by XRR analysis. The AlF_3 ALD films were also stable in air. The thickness, film density, and film roughness of AlF_3 films did not change after storage in atmosphere for one month.

AlF_3 is slightly soluble in liquid water with a solubility of 0.5 g of AlF_3 in 100 g of H_2O.[31] The change of AlF_3 ALD film thickness versus time during immersion in DI water was monitored using XRR and SE measurements. These experiments determined the etch rate of AlF_3 in liquid water at room temperature. The etch rate of the AlF_3 ALD films was extremely constant at 10 Å/h. During the etching, the density, roughness, and refractive index of the AlF_3 ALD films were almost constant. These results suggest that the AlF_3 etching in liquid water occurs by a layer-by-layer process.

IV. CONCLUSIONS

AlF_3 ALD films were grown over a range of temperatures from 75 to 300 °C using TMA and HF from HF-pyridine as the reactants. The AlF_3 ALD was examined using in situ quartz crystal microbalance (QCM), quadrupole mass spectrometer (QMS) and Fourier transform infrared (FTIR) spectroscopy. The maximum mass gain per cycle (MGPC) for AlF_3 ALD of 44 ng/(cm^2 cycle) occurred at 100 °C. The MGPC then decreased progressively at higher temperatures. The MGPC became negative at T > 250 °C. At these higher temperatures, the TMA and HF were able to etch the underlying AlF_3 films.

FTIR measurements observed an absorbance increase at 500−900 cm^{-1} during AlF_3 ALD at 150 °C. This absorbance increase was attributed to Al−F stretching vibrations in the AlF_3 ALD film. The FTIR spectra also revealed $AlF(CH_3)_2$ and HF species on the surface after the TMA and HF exposures, respectively, at 150 °C. $AlF(CH_3)_2$ is the key reaction intermediate during AlF_3 ALD. $AlF(CH_3)_2$ is fluorinated by

DOI: 10.1021/acs.jpcc.5b02625
J. Phys. Chem. C 2015, 119, 14185−14194

the HF exposure and produces AlF_3 growth. HF also adsorbs on the growing AlF_3 film and is available to form more $AlF(CH_3)_2$ during the subsequent HF exposure.

Ex situ X-ray reflectivity (XRR) and spectroscopic ellipsometry (SE) measurements were also employed to measure the AlF_3 ALD film thicknesses. The AlF_3 ALD growth rate measured by XRR and SE was 1.43 Å/cycle at 100 °C. XPS and RBS measurements showed that the AlF_3 ALD films were nearly stoichiometric AlF_3 with an oxygen impurity of only ~2 at %. GIXRD analysis revealed that the AlF_3 ALD films were amorphous. XRR measurements indicated that the AlF_3 ALD were smooth. These AlF_3 ALD films may be useful for a number of applications such as ultraviolet optical films, protective coatings for the electrodes of Li ion batteries, and Lewis acid catalytic films.

AUTHOR INFORMATION

Corresponding Author

*E-mail: steven.george@colorado.edu.

Notes

The authors declare no competing financial interest.

ACKNOWLEDGMENTS

This research was funded by the Department of Energy through the DOE-BATT program. Additional funding was provided by the National Science Foundation (CHE-1306131). The authors thank Dr. Greg Haugstad in the Nanofabrication Center at the University of Minnesota for the RBS measurements. The authors also thank Markus Neuber for the GIXRD measurements.

REFERENCES

(1) Pellicori, S. F.; Colton, E. Fluoride Compounds for IR Coatings. *Thin Solid Films* **1992**, *209*, 109−115.

(2) Staritzky, E.; Asprey, L. B. Aluminum Trifluoride, AlF_3. *Anal. Chem.* **1957**, *29*, 984−984.

(3) Barriere, A. S.; Lachter, A. Optical-Transitions in Disordered Thin-Films of Ionic Compounds MgF_2 and AlF_3 as a Function of Their Conditions of Preparation. *Appl. Opt.* **1977**, *16*, 2865−2871.

(4) Konig, D.; Scholz, R.; Zahn, D. R. T.; Ebest, G. Band Diagram of the $AlF_3/SiO_2/Si$ System. *J. Appl. Phys.* **2005**, *97*, 093707.

(5) Bridou, F.; Cuniot-Ponsard, M.; Desvignes, J. M.; Richter, M.; Kroth, U.; Gottwald, A. Experimental Determination of Optical Constants of MgF_2 and AlF_3 Thin Films in the Vacuum Ultra-Violet Wavelength Region (60−124 nm), and its Application to Optical Designs. *Opt. Commun.* **2010**, *283*, 1351−1358.

(6) Lee, C. C.; Liu, M. C.; Kaneko, M.; Nakahira, K.; Takano, Y. Characterization of AlF_3 Thin Films at 193 nm by Thermal Evaporation. *Appl. Opt.* **2005**, *44*, 7333−7338.

(7) Niisaka, S.; Saito, T.; Saito, J.; Tanaka, A.; Matsumoto, A.; Otani, M.; Biro, R.; Ouchi, C.; Hasegawa, M.; Suzuki, Y.; Sone, K. Development of Optical Coatings for 157 nm Lithography. I. Coating Materials. *Appl. Opt.* **2002**, *41*, 3242−3247.

(8) Sun, Y. K.; Lee, M. J.; Yoon, C. S.; Hassoun, J.; Amine, K.; Scrosati, B. The Role of AlF_3 Coatings in Improving Electrochemical Cycling of Li-Enriched Nickel-Manganese Oxide Electrodes for Li-Ion Batteries. *Adv. Mater.* **2012**, *24*, 1192−1196.

(9) Ding, F.; Xu, W.; Choi, D. W.; Wang, W.; Li, X. L.; Engelhard, M. H.; Chen, X. L.; Yang, Z. G.; Zhang, J. G. Enhanced Performance of Graphite Anode Materials by AlF_3 Coating for Lithium-Ion Batteries. *J. Mater. Chem.* **2012**, *22*, 12745−12751.

(10) Zheng, J. M.; Zhang, Z. R.; Wu, X. B.; Dong, Z. X.; Zhu, Z.; Yang, Y. The Effects of AlF_3 Coating on the Performance of $Li[Li_{0.2}Mn_{0.54}Ni_{0.13}Co_{0.13}]O_2$ Positive Electrode Material for Lithium-Ion Battery. *J. Electrochem. Soc.* **2008**, *155*, A775−A782.

(11) Myung, S. T.; Lee, K. S.; Yoon, C. S.; Sun, Y. K.; Amine, K.; Yashiro, H. Effect of AlF_3 Coating on Thermal Behavior of Chemically Delithiated $Li_{0.35}[Ni_{1/3}Co_{1/3}Mn_{1/3}]O_2$. *J. Phys. Chem. C* **2010**, *114*, 4710−4718.

(12) Herron, N.; Farneth, W. E. The Design and Synthesis of Heterogeneous Catalyst Systems. *Adv. Mater.* **1996**, *8*, 959−968.

(13) Kemnitz, E.; Gross, U.; Rudiger, S.; Shekar, C. S. Amorphous Metal Fluorides with Extraordinary High Surface Areas. *Angew. Chem., Int. Ed.* **2003**, *42*, 4251−4254.

(14) Kemnitz, E.; Menz, D. H. Fluorinated Metal Oxides and Metal Fluorides as Heterogeneous Catalysts. *Prog. Solid State Chem.* **1998**, *26*, 97−153.

(15) Taki, Y. Film Structure and Optical Constants of Magnetron-Sputtered Fluoride Films for Deep Ultraviolet Lithography. *Vacuum* **2004**, *74*, 431−435.

(16) Iwahori, K.; Furuta, M.; Taki, Y.; Yamamura, T.; Tanaka, A. Optical Properties of Fluoride Thin Films Deposited by RF Magnetron Sputtering. *Appl. Opt.* **2006**, *45*, 4598−4602.

(17) Heitmann, W. Vacuum Evaporated Films of Aluminum Fluoride. *Thin Solid Films* **1970**, *5*, 61−67.

(18) Targove, J. D.; Bovard, B. G.; Lingg, L. J.; Macleod, H. A. Densification of Aluminum Fluoride Thin-Films by Ion-Assisted Deposition. *Thin Solid Films* **1988**, *159*, L57−L59.

(19) George, S. M. Atomic Layer Deposition: An Overview. *Chem. Rev.* **2010**, *110*, 111−131.

(20) Lee, Y.; Cavanagh, A. S.; George, S. M. Atomic Layer Deposition of AlF_3 Using Trimethylaluminum and Hydrogen Fluoride-Pyridine. *Proceedings of the 13th International Conference on Atomic Layer Deposition*, San Diego, California, July 28−31, 2013.

(21) Mäntymäki, M.; Heikkilä, M. J.; Puukilainen, E.; Mizohata, K.; Marchand, B.; Räisänen, J.; Ritala, M.; Leskelä, M. Atomic Layer Deposition of AlF_3 Thin Films Using Halide Precursors. *Chem. Mater.* **2014**, *27*, 604−611.

(22) Elam, J. W.; Groner, M. D.; George, S. M. Viscous Flow Reactor with Quartz Crystal Microbalance for Thin Film Growth by Atomic Layer Deposition. *Rev. Sci. Instrum.* **2002**, *73*, 2981−2987.

(23) Lee, Y.; Yoon, B.; Cavanagh, A. S.; George, S. M. Molecular Layer Deposition of Aluminum Alkoxide Polymer Films Using Trimethylaluminum and Glycidol. *Langmuir* **2011**, *27*, 15155−15164.

(24) Hennessy, J.; Jewell, A. D.; Greer, F.; Lee, M. C.; Nikzad, S. Atomic Layer Deposition of Magnesium Fluoride via Bis-(ethylcyclopentadienyl)magnesium and Anhydrous Hydrogen Fluoride. *J. Vac. Sci. Technol., A* **2015**, *33*, 01A125.

(25) Olah, G. A.; Nojima, M.; Kerekes, I. Synthetic Methods and Reactions. 2. Hydrofluorination of Alkenes, Cyclopropane and Alkynes with (Trialkylamine) Reagents. *Synthesis (Stuttgart, Ger.)* **1973**, 779−780.

(26) DuMont, J. W.; George, S. M. Pyrolysis of Alucone Molecular Layer Deposition Films Studied Using In Situ Transmission Fourier Transform Infrared Spectroscopy, *J. Phys. Chem. C* **2015**, in press, 10.1021/jp512074n.

(27) Ballinger, T. H.; Wong, J. C. S.; Yates, J. T. Transmission Infrared-Spectroscopy of High Area Solid-Surfaces: A Useful Method for Sample Preparation. *Langmuir* **1992**, *8*, 1676−1678.

(28) Ferguson, J. D.; Weimer, A. W.; George, S. M. Atomic Layer Deposition of Al_2O_3 Films on Polyethylene Particles. *Chem. Mater.* **2004**, *16*, 5602−5609.

(29) Shannon, R. D.; Shannon, R. C.; Medenbach, O.; Fischer, R. X. Refractive Index and Dispersion of Fluorides and Oxides. *J. Phys. Chem. Ref. Data* **2002**, *31*, 931−970.

(30) Lennard, W. N. *QUARK* v. 1.3, 2001, http://www.physics.uwo.ca/~wlennard (accessed May 21, 2015).

(31) *CRC Handbook of Chemistry and Physics*, 85th ed.; Lide, D. R., Ed.; CRC Press: Boca Raton, FL, 2005.

(32) Linstrom, P. J.; Mallard, W. G. *NIST Chemistry WebBook, NIST Standard Reference Database Number 69*, National Institute of Standards and Technology: Gaithersburg, MD, http://webbook.nist.gov (accessed May 21, 2015).

DOI: 10.1021/acs.jpcc.5b02625
J. Phys. Chem. C 2015, 119, 14185−14194

(33) van der Meulen, P. A.; Mann, R. F. The Vapor Pressure of Pyridine. *J. Am. Chem. Soc.* **1931**, *53*, 451−453.
(34) Atkins, P. W. *Physical Chemistry*, 5th ed.; Oxford University Press: Oxford, 1994.
(35) Ott, A. W.; Klaus, J. W.; Johnson, J. M.; George, S. M. Al_3O_2 Thin Film Growth on Si(100) using Binary Reaction Sequence Chemistry. *Thin Solid Films* **1997**, *292*, 135−144.
(36) Lee, Y.; DuMont, J. W.; George, S. M. Atomic Layer Etching of HfO_2 Using Sequential, Self-Limiting Thermal Reactions with $Sn(acac)_2$ and HF. *ECS J. Solid State Sci. Technol.* **2015**, *4*, N5013−N5022.
(37) Lee, Y.; George, S. M. Atomic Layer Etching of Al_2O_3 Using Sequential, Self-Limiting Thermal Reactions with $Sn(acac)_2$ and HF. *ACS Nano* **2015**, *9*, 2061−2070.
(38) Gross, U.; Ruediger, S.; Kemnitz, E.; Brzezinka, K.-W.; Mukhopadhyay, S.; Bailey, C. Wander, A.; Harrison, N., Vibrational Analysis Study of Aluminum Trifluoride Phases. *J. Phys. Chem. A* **2007**, *111*, 5813−5819.
(39) Koenig, R.; Scholz, G.; Scheurell, K.; Heidemann, D.; Buchem, I.; Unger, W. E. S.; Kemnitz, E. Spectroscopic Characterization of Crystalline AlF_3 Phases. *J. Fluorine Chem.* **2010**, *131*, 91−97.
(40) Utkin, A. N.; Girichev, G. V.; Giricheva, N. I.; Khaustov, S. V. Structure and Vibrational Frequencies of Aluminum Trifluoride and Gallium Trifluoride. *J. Struct. Chem.* **1986**, *27*, 212−215.
(41) Kinney, J. B.; Staley, R. H. Reactions of Titanium Tetrachloride and Trimethylaluminum at Silica Surfaces Studied by Using Infrared Photo-Acoustic Spectroscopy. *J. Phys. Chem.* **1983**, *87*, 3735−3740.
(42) Giguere, P. A.; Zengin, N. Spectre Infrarouge de HF a L'etat Cristallin. *Can. J. Chem.* **1958**, *36*, 1013−1019.
(43) Tse, W. S.; Anderson, A.; Torrie, B. H. Infrared Spectra of Crystalline HF and DF. *Annu. Rep. Inst. Phys., Acad. Sin.* **1981**, *11*, 13−22.
(44) Wang, P. F.; Ding, S. J.; Zhang, W.; Zhang, J. Y.; Wang, J. T.; Wei, W. L. FTIR Characterization of Fluorine Doped Silicon Dioxide Thin Films Deposited by Plasma Enhanced Chemical Vapor Deposition. *Chin. Phys. Lett.* **2000**, *17*, 912−914.
(45) Weidlein, J.; Krieg, V. Vibrational Spectra of Dimethyl and Diethyl Aluminum Fluoride. *J. Organomet. Chem.* **1968**, *11*, 9−16.
(46) Ayotte, P.; Hebert, M.; Marchand, P. Why is Hydrofluoric Acid a Weak Acid? *J. Chem. Phys.* **2005**, *123*, 184501.
(47) Bailey, C. L.; Wander, A.; Mukhopadhyay, S.; Searle, B. G.; Harrison, N. M. Adsorption of HF and HCl on the beta-AlF_3 (100) Surface. *Phys. Chem. Chem. Phys.* **2008**, *10*, 2918−2924.
(48) Bailey, C. L.; Mukhopadhyay, S.; Wander, A.; Searle, B. G.; Harrison, N. M. Structure and Stability of alpha-AlF_3 Surfaces. *J. Phys. Chem. C* **2009**, *113*, 4976−4983.
(49) Pulker, H. K. Characterization of Optical Thin Films. *Appl. Opt.* **1979**, *18*, 1969−1977.

DOI: 10.1021/acs.jpcc.5b02625
J. Phys. Chem. C 2015, 119, 14185−14194